第41卷第2期
2022年4月

红外与毫米波学报
J. Infrared Millim. Waves

Vol. 41，No. 2
April，2022

文章编号：1001-9014(2022)02-0384-05

DOI：10. 11972/j. issn. 1001-9014. 2022. 02. 002

Interfacial properties between Al_2O_3 and $In_{0.74}Al_{0.26}As$ epitaxial layer on MIS capacitors

WAN Lu-Hong[1,2,3]， SHAO Xiu-Mei[1,2*]， LI Xue[1,2*]， GU Yi[1,2]， MA Ying-Jie[1,2]， LI Tao[1,2]

(1. State Key Laboratories of Transducer Technology，Shanghai Institute of Technical Physics，Chinese Academy of Sciences，Shanghai 200083，China；
2. Key Laboratory of Infrared Imaging Materials and Detectors，Shanghai Institute of Technical Physics，Chinese Academy of Sciences，Shanghai 200083，China；
3. University of Chinese Academy of Sciences，Beijing 100049，China)

Abstract：Metal-Insulator-Semiconductor (MIS) capacitors were fabricated on $In_{0.74}Al_{0.26}As/In_{0.74}Ga_{0.26}As/In_xAl_{1-x}As$ heterostructure multilayer semiconductor materials. SiN_x and SiN_x/Al_2O_3 bilayer were applied as insulating layer to prepare MIS capacitors respectively. High-resolution transmission electron microscopy (HRTEM) and X-ray photoelectron spectroscopy (XPS) measurements indicated that，compared with SiN_x deposited by inductively coupled plasma chemical vapor deposition (ICPCVD)，Al_2O_3 deposited by atomic layer deposition (ALD) can effectively suppresses In_2O_3 at the interface between Al_2O_3 and $In_{0.74}Al_{0.26}As$. According to the capacitance-voltage (C-V) measurement result of MIS capacitors，the fast interface state density (D_{it}) of $SiN_x/Al_2O_3/In_{0.74}Al_{0.26}As$ was one order of magnitude lower than that of $SiN_x/In_{0.74}Al_{0.26}As$. Therefore，it can be concluded that Al_2O_3 deposited by ALD as a passivation film can effectively reduce the interface state density between Al_2O_3 and $In_{0.74}Al_{0.26}As$，thereby reducing the dark current of p-$In_{0.74}Al_{0.26}As$/i-$In_{0.76}Ga_{0.24}As$/n-$In_xAl_{1-x}As$ photodiodes.

Key words：InAlAs，ALD，Al_2O_3，SiN_x，MIS capacitor，interface state density
PACS: 73.90.+f

基于MIS电容器的Al_2O_3与$In_{0.74}Al_{0.26}As$的界面特性

万露红[1,2,3]， 邵秀梅[1,2*]， 李　雪[1,2*]， 顾　溢[1,2]， 马英杰[1,2]， 李　淘[1,2]

(1. 中国科学院上海技术物理研究所 传感器技术国家重点实验室，上海200083；
2. 中国科学院上海技术物理研究所 红外成像材料与器件重点实验室，上海200083；
3. 中国科学院大学，北京100049)

摘要：采用$In_{0.74}Al_{0.26}As$ / $In_{0.74}Ga_{0.26}As$ / $In_xAl_{1-x}As$异质结构多层半导体作为半导体层，制备了金属-绝缘体-半导体(MIS)电容器。其中，SiN_x和SiN_x / Al_2O_3分别作为MIS电容器的绝缘层。高分辨率透射电子显微镜和X射线光电子能谱的测试结果表明，与通过电感耦合等离子体化学气相沉积生长的SiN_x相比，通过原子层沉积生长的Al_2O_3可以有效地抑制Al_2O_3和$In_{0.74}Al_{0.26}As$界面的In_2O_3的含量。根据MIS电容器的电容-电压测量结果，计算得到SiN_x / Al_2O_3 / $In_{0.74}Al_{0.26}As$的快界面态密度比SiN_x / $In_{0.74}Al_{0.26}As$的快界面态密度低一个数量级。因此，采用原子层沉积生长的Al_2O_3作为钝化膜可以有效地降低Al_2O_3和$In_{0.74}Al_{0.26}As$之间的快界面态密度，从而降低$In_{0.74}Ga_{0.26}As$探测器的暗电流。

关　键　词：InAlAs；原子层沉积；Al_2O_3；SiN_x；金属-绝缘体-半导体电容器；界面态密度

Introduction

InGaAs photodiodes are very promising and have been widely used in short wavelength infrared (SWIR) detection [1-2]. The defects caused by the lattice mismatch between $In_{0.74}Ga_{0.26}As$ and InP substrate is inevitable. In order to improve the performance of $In_{0.74}Ga_{0.26}As$ photodiodes，it is necessary to optimize the epilayer and manufacturing processes of the InGaAs photodiodes. The dark

Received date：2021-04-10，**revised date**：2022-01-27　　**收稿日期**：2021-04-10，**修回日期**：2022-01-27
Foundation items：Supported by National Natural Science Foundation of China (61704180，62175250)
Biography：WAN Lu-Hong (1993-)，female，Jiangxi，China，Ph. D. Research area involves short wavelength infrared photodiodes. E-mail：wanluhong_wan@163. com
* **Corresponding author**：E-mail：shaoxm@mail. sitp. ac. cn，lixue@mail. sitp. ac. cn

current of the mesa $In_{0.74}Ga_{0.26}As$ photodiodes is composed of body dark current and side dark current [3]. Passivation is one of the key processes of the mesa PIN photodiodes. Therefore, it is essential to optimize the passivation to reduce the dark current of the mesa $In_{0.74}Al_{0.26}As$ (p)/$In_{0.74}Ga_{0.26}As$(i)/$In_xAl_{1-x}As$(n) photodiodes.

As an outstanding thin film deposition technology, ALD has broad prospects in semiconductor device fabrication [4-6]. ALD involves two self-limiting surface reactions in which the growth substrate is exposed to alternating pulses of co-reactant and precursor [7-8]. Therefore, ALD can precisely control the thickness of thin film with an accuracy of an atomic layer. Moreover, films deposited by ALD are dense and of high quality. In our previous work, Al_2O_3 deposited by ALD has been proved to be an effective passivation film in $In_{0.74}Ga_{0.26}As$ photodiodes [9-10]. However, the reason why the ALD-Al_2O_3 reduces the dark current of $In_{0.74}Ga_{0.26}As$ photodiodes has not been explored. Therefore, it is necessary to study the interface state density between ALD-Al_2O_3 and $In_{0.74}Al_{0.26}As$ layer.

In this paper, TEM and XPS measurements were performed to investigate the interface between two different dielectric films and $In_{0.74}Al_{0.26}As$ layer. The two different dielectric films were ALD-Al_2O_3 and ICPCVD-SiN_x respectively. In addition, MIS capacitors have been prepared by using above two dielectric films to further quantitatively study the interface state density between dielectric film and $In_{0.74}Al_{0.26}As$ layer.

1 Experimental details

To investigate the interface state density of SiN_x/$In_{0.74}Al_{0.26}As$ and SiN_x/Al_2O_3/ $In_{0.74}Al_{0.26}As$, two series of MIS capacitor were prepared. The SiN_x or Al_2O_3 were deposited on the $In_{0.74}Al_{0.26}As$/$In_{0.74}Ga_{0.26}As$/$In_xAl_{1-x}As$ heterostructures that were grown on an InP substrate by gas source molecular beam epitaxy (MBE) [11]. What's more, the materials used to prepare the samples were cleaved from the same wafer. To remove surface native oxide layer, the wafer involved in this paper were treated with hydrofluoric acid buffer solution before film deposition.

TEM and XPS measurements were employed to investigate the interface between films and $In_{0.74}Al_{0.26}As$ layer. The 20-nm-thick Al_2O_3 films were deposited on $In_{0.74}Al_{0.26}As$ by 220 cycles of trimethylaluminum (TMA) and H_2O at 150°C for the TEM and XPS measurements. For comparison purpose, about 20-nm-thick SiN_x films were deposited on $In_{0.74}Al_{0.26}As$ by ICPCVD of SiH_4 and N_2 at 75°C for the TEM and XPS measurements. Furthermore, bare $In_{0.74}Al_{0.26}As$ wafer with native oxides was used as a control for XPS measurement. The insulator of sample A was deposited with 135-nm-thick SiN_x film by ICPCVD. The insulator of sample B is ICPCVD-SiN_x/ALD-Al_2O_3 bilayer, where 20-nm-thick Al_2O_3 was firstly deposited by ALD and 130-nm-thick SiN_x was then deposited by ICPCVD. Fig. 1(a) shows the sectional schematic of MIS capacitors. The dielectric film of sample A and sample B were SiN_x film and SiN_x/Al_2O_3 bilayer respectively. The photography of MIS capacitor was represented in Fig. 1(b). The C-V characteristics of MIS capacitors at different frequencies were measured by Agilent B1500A Semiconductor Device Analyzer.

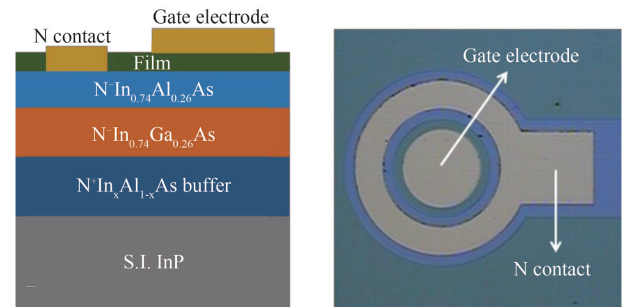

Fig. 1 (a) Sectional schematic diagram and (b) photography of MIS capacitor
图1 MIS电容器的(a)截面示意图,(b)电子显微图像

2 Results and discussion

Pt was firstly deposited on the surface of $In_{0.74}Al_{0.26}As$ wafer to protect the wafer from etching damage. Focused Ion Beam (FIB) was used to thin the sample, and then the thinned sample was subjected to TEM testing. The cross-section TEM images of ICPCVD-SiN_x/$In_{0.74}Al_{0.26}As$ and ALD-Al_2O_3/$In_{0.74}Al_{0.26}As$ structure were shown in Fig. 2 (top). In comparison with SiN_x/$In_{0.74}Al_{0.26}As$, a sharp transition from Al_2O_3 to $In_{0.74}Al_{0.26}As$ can be observed. In addition, the cross-sectional composition information of Fig. 2 (bottom) obtained by Energy Dispersive X-ray Spectroscopy (EDS) can also illustrate this. The transition from SiN_x to $In_{0.74}Al_{0.26}As$ layer was ~5 nm, while the transition from Al_2O_3 to $In_{0.74}Al_{0.26}As$ layer was ~3 nm.

In order to further study the interface state density between film and $In_{0.74}Al_{0.26}As$, XPS test combined with Ar^+ sputtering (2 kV, 20 μA) was utilized. XPS spectra were obtained with the Axis UltraDLD spectrometer (Kratos Analytical-A Shimadzu Group Company) with a monochromatic Al Kα source ($h\nu$=1486.6 eV) and a charge neutralization system. The spectra were taken when the vacuum of the analysis chamber was less than 5×10^{-9} Torr. The electron energy analyzer works in the hybrid magnification mode, and the take-off angle for the analyzer relative to sample surface is 90°. The X-ray source power was set to 105 W (15 kV, 7 mA) for high-resolution spectra acquisition. The pass energy of 40 eV were utilized for narrow scan spectra. The energy step size of 0.1 eV were chosen for narrow scan spectra. The C 1s peak of environmental pollution carbon adsorbed on the sample surface is used as the reference peak for spectral energy correction to complete the peak position calibration: set the C 1s peak position of the pollution carbon to 284.8 eV. Calculate the relative percentage of elements through the peak area of the element peak and the sensitivity factor of the instrument.

$In3d_{5/2}$ spectra obtained by XPS narrow scan was shown in Fig. 3. As shown in Fig. 3(a), there was a

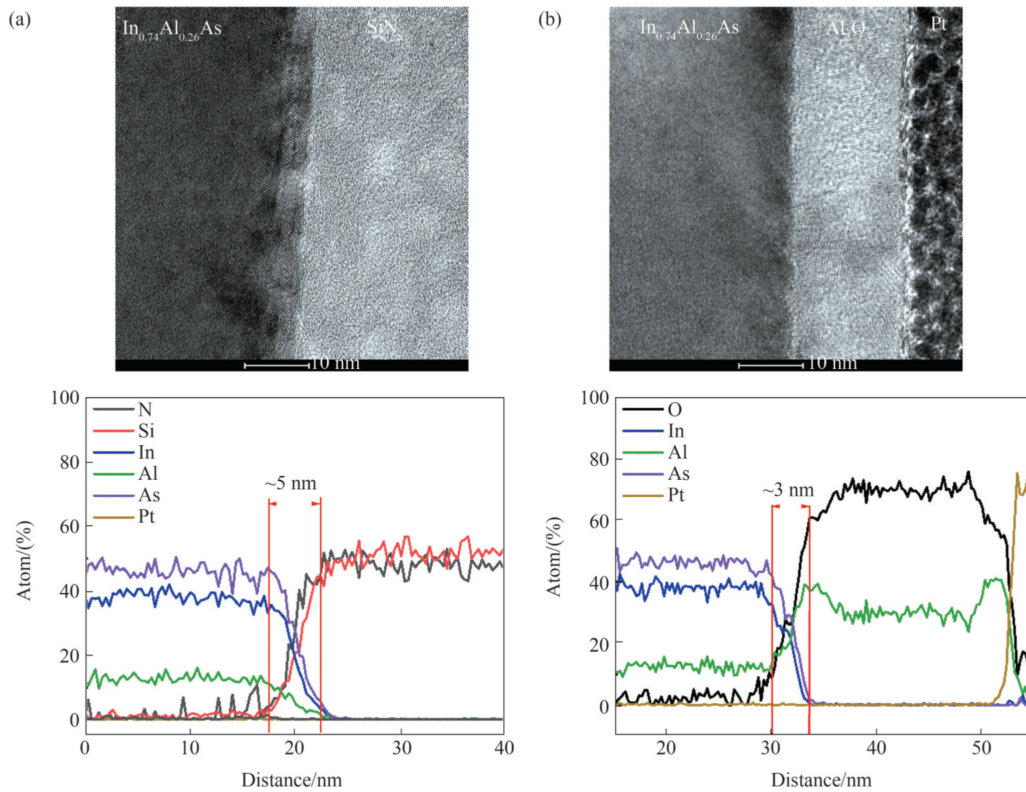

Fig. 2 The cross-sectional images (top) obtained by TEM and cross-sectional composition information (bottom) obtained by EDS of (a) ICPCVD-SiN_x on $In_{0.74}Al_{0.26}As$ and (b) ALD-Al_2O_3 on $In_{0.74}Al_{0.26}As$

图2 通过TEM测试得到的横截面图像(顶部)和通过EDS获得的横截面组成信息(底部)(a) ICPCVD-SiN_x on $In_{0.74}Al_{0.26}As$ 和(b) ALD-Al_2O_3 on $In_{0.74}Al_{0.26}As$

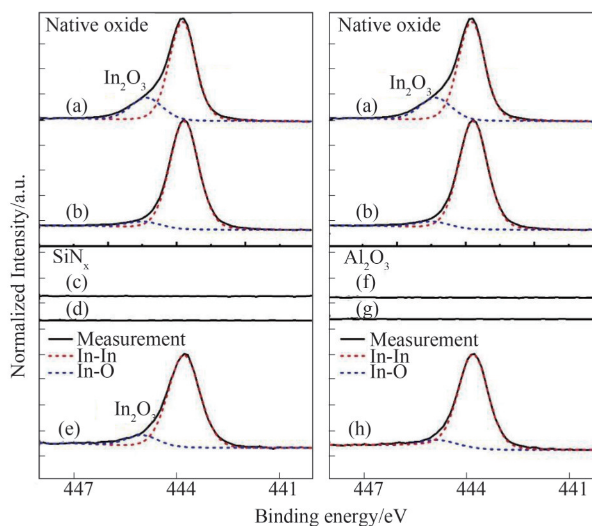

Fig. 3 The $3d_{5/2}$ core level of In recorded from bare $In_{0.74}Al_{0.26}As$ wafer, ICPCVD-SiN_x/$In_{0.74}Al_{0.26}As$ and ALD-Al_2O_3/$In_{0.74}Al_{0.26}As$ (a) on the surface of bare $In_{0.74}Al_{0.26}As$, (b) in the bulk of $In_{0.74}Al_{0.26}As$, (c) on the surface of ICPCVD-SiN_x, (d) in the bulk of ICPCVD-SiN_x, (e) at the interface between ICPCVD-SiN_x and $In_{0.74}Al_{0.26}As$, (f) on the surface of ALD-Al_2O_3, (g) in the bulk of ALD-Al_2O_3, and (h) at the interface between ALD-Al_2O_3 and $In_{0.74}Al_{0.26}As$

图3 测试得到的In的$3d_{5/2}$能谱图 (a) 裸露的$In_{0.74}Al_{0.26}As$表面,(b) 裸露的$In_{0.74}Al_{0.26}As$层,(c) ICPCVD-SiNx/$In_{0.74}Al_{0.26}As$的SiN_x表面,(d) ICPCVD-SiN_x/$In_{0.74}Al_{0.26}As$的SiN_x层,(e) ICPCVD-SiN_x/$In_{0.74}Al_{0.26}As$的界面,(f) ALD-Al_2O_3/$In_{0.74}Al_{0.26}As$的Al_2O_3表面,(g) ALD-Al_2O_3/$In_{0.74}Al_{0.26}As$的Al_2O_3层,(h) ALD-Al_2O_3/$In_{0.74}Al_{0.26}As$的界面

certain amount of In_2O_3 on the surface of the bare $In_{0.74}Al_{0.26}As$ wafer. Compared with the surface of bare $In_{0.74}Al_{0.26}As$ wafer, almost no In_2O_3 could be found in the bulk of $In_{0.74}Al_{0.26}As$ [Fig. 3(b)]. The amount of In_2O_3 at the SiN_x/$In_{0.74}Al_{0.26}As$ interface [Fig. 3(e)] was less than that of the surface of bare $In_{0.74}Al_{0.26}As$ wafer. However,

there was still a certain amount of In_2O_3 at the SiN_x/$In_{0.74}Al_{0.26}As$ interface that couldn't be ignored. Thus, ICPCVD-SiN_x film could reduce part of In_2O_3 at the interface between SiN_x and $In_{0.74}Al_{0.26}As$. The interface between Al_2O_3/$In_{0.74}Al_{0.26}As$ [Fig. 3(h)] was equivalent to the bulk of $In_{0.74}Al_{0.26}As$, and there was almost no In_2O_3 could be found at the interface between Al_2O_3 and $In_{0.74}Al_{0.26}As$. Therefore, it can be concluded that ALD-Al_2O_3 can effectively suppress the In_2O_3 at the interface between film and $In_{0.74}Al_{0.26}As$.

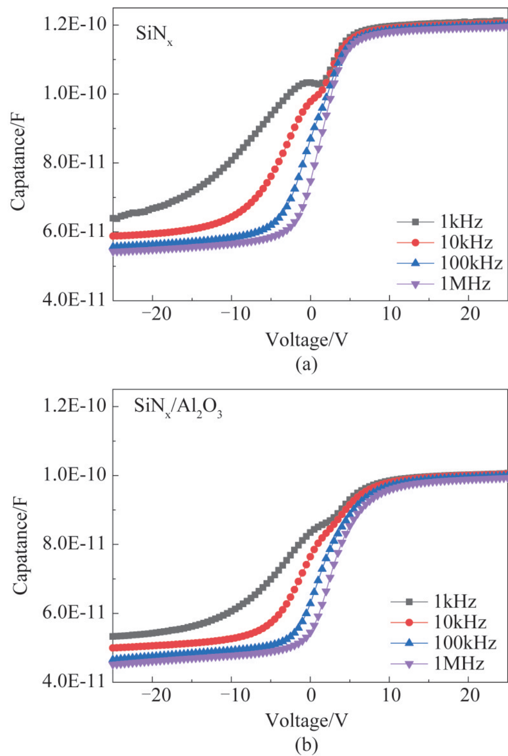

Fig. 4 *C-V* curves of MIS capacitors measured at 210 K for different frequencies from 1 kHz to 1 MHz (a) SiN_x/$In_{0.74}Al_{0.26}As$ MIS capacitor, (b) SiN_x/Al_2O_3 $In_{0.74}Al_{0.26}As$ MIS capacitor
图4 不同测试频率下的MIS电容器的*C-V*曲线(210 K)(a) SiN_x/$In_{0.74}Al_{0.26}As$ MIS电容器,(b) SiN_x/Al_2O_3 $In_{0.74}Al_{0.26}As$ MIS电容器。

Figure 4 shows the *C-V* curves of SiN_x/$In_{0.74}Al_{0.26}As$ and SiN_x/Al_2O_3/$In_{0.74}Al_{0.26}As$ MIS capacitors with bias voltage from 25 V to -25 V at 210 K. The *C-V* measurements of these capacitors was performed with frequency varying from 1 kHz to 1 MHz. Under the low frequency limit, the capacitance of MIS capacitor (C_{LF}) was equivalent to the parallel connection of semiconductor capacitance (C_s) and interface trap capacitance (C_{it}) and then the series connection of insulating layer capacitance (C_i). Therefore, the C_{LF} can be expressed as:

$$\frac{1}{C_{LF}} = \frac{1}{C_s + C_{it}} + \frac{1}{C_i} \quad . \quad (1)$$

However, under the high frequency limit, the interface trapped charge can not keep up with the change of high frequency. Therefore, the capacitance of MIS capacitor (C_{HF}) was equivalent to the series connection of semiconductor capacitance (C_s) and insulating layer capacitance (C_i). Thus, the C_{HF} can be expressed as:

$$\frac{1}{C_{HF}} = \frac{1}{C_s} + \frac{1}{C_i} \quad . \quad (2)$$

According to Eqs (1-2), the fast interface state density (D_{it}) can be expressed as (high-low frequency method)[12-13]:

$$D_{it} = \frac{C_{it}}{q^2} = \frac{C_i}{qA}\left(\frac{C_{LF}}{C_i - C_{LF}} - \frac{C_{HF}}{C_i - C_{HF}}\right) \quad , \quad (3)$$

where A is the area of gate electrode.

In this paper, the C_{LF} was the capacitance of MIS capacitor under 1 kHz, while the C_{HF} was the capacitance of MIS capacitor under 1 MHz. The D_{it} values of sample A and B were 2.29×10^{13} $cm^{-2}eV^{-1}$ and 1.83×10^{12} $cm^{-2}eV^{-1}$ respectively, which were calculated by high-low frequency method. Apparently, the calculated D_{it} of sample B is an order of magnitude smaller than that of sample A. Thus, ALD-Al_2O_3 effectively reduces the D_{it} between Al_2O_3 and $In_{0.74}Al_{0.26}As$. This can be explained by the growth of Al_2O_3 deposited by ALD. Firstly, an aluminum source is introduced to effectively neutralize the dangling bonds on the surface of $In_{0.74}Al_{0.26}As$, and then a water source is introduced to form a bond with aluminum. Therefore, the interface state density (such as In_2O_3) between the dielectric film and $In_{0.74}Al_{0.26}As$ is effectively reduced.

Combining the XPS test and the *C-V* measurement results of the MIS capacitors, it can be concluded that ALD-Al_2O_3 effectively reduces the fast interface state density between the film and the $In_{0.74}Al_{0.26}As$. Therefore, the lower 1/f noise and dark current density characteristics of $In_{0.74}Ga_{0.26}As$ photodiodes passivated by SiN_x/Al_2O_3 bilayer [9-10] are attributed to the lower fast interface state density between the film and the $In_{0.74}Al_{0.26}As$.

3 Conclusion

According to the study of the interface between dielectric film and $In_{0.74}Al_{0.26}As$, it is found that the interface between the ALD-Al_2O_3 and $In_{0.74}Al_{0.26}As$ is sharper than that of ICPCVD-SiN_x and $In_{0.74}Al_{0.26}As$. In addition, ALD-Al_2O_3 effectively reduces the In_2O_3 at the interface between ALD-Al_2O_3 and $In_{0.74}Al_{0.26}As$. Furthermore, the C-V results of the MIS capacitors also indicate that the ALD-Al_2O_3 effectively reduces the fast interface state density of the dielectric film and $In_{0.74}Al_{0.26}As$. In summary, using ALD-Al_2O_3 as the passivation film of the $In_{0.74}Ga_{0.26}As$ photodiodes can theoretically reduce the dark current of the $In_{0.74}Ga_{0.26}As$ photodiodes. Furthermore, the device verification results have confirmed this statement.

References

[1] Huang C, Ho C L, Wu M C. Large-area planar wavelength extended InGaAs p-i-n photodiodes using rapid thermal diffusion with spin-on dopant technique[J]. *IEEE Electron Device Lett*. 2015, **36**(8): 820-822.

[2] Li X, Gong H, Fang J X, *et al*. The development of InGaAs short wavelength infrared focal plane arrays with high performance[J]. *Infrared Physics and Technol*. 2017, **80**: 112-119.

[3] Rouvié A, Reverchon J L, Huet O, *et al*. InGaAs focal plane array

developments at III-V Lab[J]. *Proc. SPIE*, 2012, **8353**:835308.
[4] Sneh O, Clark-Phelps R B, Londergan A R, *et al*. Thin film atomic layer deposition equipment for semiconductor processing [J]. *Thin Solid Films 2002*, 402:248-261.
[5] Palmstrom A F, Santra P K, Bent S F. Atomic layer deposition in nanostructured photovoltaics: Tuning optical, electronic and surface properties[J]. *Nanoscale*, 2015, **7**(29):12266-12283.
[6] Dasgupta N P, Meng X B, Elam J W, *et al*. Atomic layer deposition of metal sulfide materials [J]. *Acc. Chem. Res.* 2015, **48** (2): 341-348.
[7] Zhou L, Bo B X, Yan X Z, *et al*. Brief review of surface passivation on III-V semiconductor[J]. *Crystals* 2018, **8**(5):226.
[8] Leskela M, Mattinen M, Ritala M. Review Article Atomic layer deposition of optoelectronic materials[J]. *J. Vac. Sci. Technol*. B 2019, **37**: 030801.
[9] Wan L H, Cao G Q, Shao X M, *et al*. High performance $In_{0.83}Ga_{0.17}As$ SWIR photodiode passivated by Al_2O_3/SiN_x stacks with low-stress SiN_x films[J]. *J. Appl. Phys*. 2019, **126**:033101.
[10] Wan L H, Shao X M, Ma Y J, *et al*. Dark current and 1/f noise characteristics of $In_{0.74}Ga_{0.26}As$ photodiode passivated by SiN_x/Al_2O_3 bilayer[J]. *Infrared Physics and Technol*. 2020, **109**:103389.
[11] Zhang Y G, Gu Y, Zhu C, *et al*. Gas source MBE grown wavelength extended 2.2 and 2.5 μm InGaAs PIN photodetectors[J]. *Infrared Phys. Technol*. 2006, **47**:257-262.
[12] Engel-Herbert R, Hwang Y, Stemmer S. Comparison of methods to quantify interface trap densities at dielectric/III-V semiconductor interfaces[J]. *J. Appl. Phys*. 2010, **108**:124101.
[13] Castagné R, Vapaille A. Description of the SiO_2-Si interface properties by means of vary low frequency MOS capacitance measurements [J]. *Surf. Sci*. 1971, **28**:157.